Proceedings of the
8th International Conference on Mechanical Engineering and Renewable Energy 2025
(ICMERE2025) 10-12 November 2025,Chattogram, Bangladesh

SciEn Conference Series: Engineering Vol. 4, 2026, pp 135-141 https://doi.org/10.38032/scse.2026.4.65

Computational Analysis of Aerodynamic Performance in Conventional and Bio-Inspired Tubercled Aircraft Wings

Mehrab Hossen, Sifat Perves and Farhan Sadik Rafi*

Department of Aeronautical Engineering, Military Institute of Science and Technology (MIST), Dhaka, Bangladesh

ABSTRACT

This research undertakes a computational fluid dynamics (CFD) simulation of the aerodynamic effectiveness of a standard NACA 2412 wing and one of its modifications, which is bio-inspired and has a tubercled leading edge. Fluent steady-state simulations with 20 m/s and 30 m/s freestream velocities and a range of -6° to 24° angles of attack were analyzed through the k–ω SST turbulence model. Results show that although the conventional wing outperforms the modified wing at lower to moderate angles of attack, the tubercled configuration significantly improves post-stall performance, leading to delayed stall and drag reduction of up to 45% at high angles of attack. Unlike the baseline wing, the tubercled wing's lift-to-drag ratio surpasses 20 even after a 15° angle of attack at 30 m/s. Structural studies show the altered pressure distributions resulted in a 20–21% increase in maximum deformation. The results reinforce the aerodynamic advantages of tubercled leading edges in agility and stall resistance, while showing the need for aeroelastic design optimization to control excessive deformation.

Keywords: Bio-Inspired Aerodynamics, Tubercled Leading Edge, Naca 2412, Stall Delay, Cfd Simulation.

1. Introduction

Enhancing aircraft wing aerodynamic efficiency has motivated innovations in active and passive flow control methods. Bio-inspired modifications, particularly tubercled leading edges emulating humpback whale flippers, have gained attention for enhancing lift, postponing stall, and increasing maneuverability . The NACA 2412 airfoil serves as an excellent foundation for investigations due to its extensive utilization and documented aerodynamic characteristics.[1][2][3]

Leading-edge tubercles are sinusoidal or spherical protrusions along the wing's anterior margin. The flow along the surface is disrupted spanwise, resulting in streamwise vortices that promote mixing within the boundary layer, inhibit large-scale flow separation, and delay stall. This leads to a smoother post-stall condition, improved lift-to-drag ratios at high angles of attack, and better lift. Tubercled wings have been reported to have a slightly reduced pre-stall lift; however, the post-stall lift is consistently better along with a higher maximum lift coefficient and a more delayed stall. The design of the wings tubercle amplitude and wavelength are key. Optimal designs enhance lift by 53% and significantly reduce drag at elevated angles of attack.[3][4][5][6][7][8]

For biomimetic design, the marine mammal's evolutionary design is taken into consideration; the structural design of the flippers allows marine mammals to navigate turbulent waters with great agility and effectiveness. This has been positive for the aviation and wind turbine industries, in which flow regulation and stall management are crucial. The use of CFD and wind tunnel tests has made it possible to describe the flow structures at the leading edge of the tubercled wing in great detail, including counter-rotating vortex pairs, localized laminar flow separation bubbles, and other aspects of flow that provide positive aerodynamic performance.[2][6][9][10][1][3]

The purpose of this research was to address the modifications' aerodynamic effects through numerical analysis to inform the design and performance enhancement of future aircraft wings.

2. Literature Review

Especially in aircraft engineering, tubercles on the leading-edge of aircraft wing designs, particularly those aerodynamically inspired by the tubercled configuration on humpback whale flippers leading to bio-aerodynamic designs, have been receiving increasing attention to achieve the goal of improving aircraft aerodynamics. These leading edge bumps provide positive results for lift increase, stall delay, and overall reduction of flow turbulence.

2.1 Aerodynamic Benefits of Leading-Edge Tubercles

Use of tubercles on aircraft wings planforms have been shown to be of benefit of aerodynamics. Gopinathan and Rose established that tubercled wings shape the flow control with the creation of vortex systems that not only defer stall but also enhance lift performance during and after stall.In sweptback wings with tubercles, they found significant gains in lift-to-drag ratios and post-stall characteristics at higher angles of attack. This aligns with Lu et al.'s study showing lift enhancements. demonstrated that optimized tubercled designs could augment stall angle and lift (53% improvement across attack angles versus smooth wings).[1][11]

*Corresponding Author Email Address: mhossen.2031@gmail.com Published By: SciEn Publishing Group

2.2 Impact of Tubercles on Stall and Flow Separation

The most important benefit of tubercled wings is stall delay, improving aircraft agility and control during high-speed or high-angle-of-attack maneuvers. Reports by Gopinathan and Rose, plus McKegney et al.,suggest that tubercles increase the angle of attack. control tubercled wings provided during and after stall is substantial. With softer stall characteristics tubercled wings are exemplary in performance during and after stall.[3][11][12]

2.3 Design Optimization and CFD Analysis

Tubercled leading edge characteristics depend on critical parameters: tubercle amplitude and wavelength. Using CFD, successfully fine-tuned these parameters for significant aerodynamic efficiency enhancement. Gopinathan and Rose used wind tunnel experiments with CFD simulations to examine these effects, emphasizing proper alignment for maximum gains.[5][11]

Bio-inspired leading-edge tubercles represent a promising approach for aircraft wing aerodynamic efficiency. By delaying stall, providing additional lift, and reducing drag at high angles of attack, they constitute an important design modification for increasing aircraft stability and maneuverability.[2]

3. Methodology

3.1 Wing Design and Modeling

Wing designs-a smooth and a tubercled version with sinusoidal leading-edge bumps-in SolidWorks used the NACA 2412 profile, then exported to ANSYS Fluent for CFD simulation of their aerodynamic performance.

1. **Conventional Wing:** The baseline configuration for the straight conventional wing was a straight, tapered wing planform with a NACA 2412 airfoil.
2. **Tubercled Leading-Edge Wing:** The sinusoidal tubercles on the altered wing were located along the leading edge.

Completed wing shapes were then imported from SolidWorks into an ANSYS Fluent CFD simulation to determine the flow characteristics of both wings.

3.2 Governing Equations

3.2.1 Aerodynamic Equations

The airflow is described by the incompressible continuity and Navier–Stokes equations, which enforce conservation of mass and momentum. Continuity requires that the divergence of the velocity field V is zero, ensuring no artificial mass sources:

$$\nabla \cdot V = 0$$

The Navier–Stokes momentum equation balances the rate of change of fluid momentum and convective transport against pressure gradients, viscous stresses, and body forces:

$$\rho(\frac{\partial V}{\partial t} + V \cdot \nabla V) = -\nabla p + \nabla \cdot \tau + \rho\, g$$

Here, ρ is fluid density, p the pressure, τ the viscous stress tensor, and g gravitational acceleration. Turbulence is accounted for via the k–ω SST model, which solves separate transport equations for turbulent kinetic energy (k) and specific dissipation rate (ω), blending the robust free-stream behavior of k–ω with the near-wall accuracy of k–ϵ. Aerodynamic forces on the wing are non-dimensionalized into lift and drag coefficients:

$$C_L = \frac{L}{\frac{1}{2}\,\rho\, V_\infty^2\, S}, C_D = \frac{D}{\frac{1}{2}\,\rho\, V_\infty^2\, S}$$

where L and D are the lift and drag forces, V_∞ the freestream velocity, and S the wing planform area.

3.2.2 Structural Equations

The wing's structural response under aerodynamic loading is governed by linear elasticity. Equilibrium requires the divergence of the stress tensor σ plus any body forces f to vanish:

$$\nabla \cdot \sigma + f = 0$$

We assume small deformations and linear material behavior, so stress and strain are related by Hooke's law:

$$\sigma = C\!:\!\varepsilon \;with\; \varepsilon = \frac{1}{2}(\nabla u + (\nabla u)^T)$$

Here, u is the displacement vector and C the fourth-order elasticity tensor defined by Young's modulus and Poisson's ratio for PLA Plus. Aerodynamic surface pressures $p(x)$ extracted from CFD are applied as traction boundary conditions:

$$\sigma \cdot n = p(x)\, n$$

This formulation allows evaluation of nodal displacements and von Mises stress under the applied pressure loads.

3.3 Computational Fluid Dynamics (CFD) Simulation

Under ANSYS Fluent, two configurations of wings (conventional and tubercled) were modeled and tested in subsonic conditions.

1. **Mesh Generation:** : Structured, fine mesh through ANSYS Meshing, with refined cells near leading and trailing edges to capture boundary-layer effects for Structured mesh generation.
2. **Boundary Conditions:**The following boundary conditions were kept the same across all the simulations:
   - Inlet:Velocity inlets at 20 m/s and 30 m/s.
   - Outlet: : Unrestricted pressure outlet.
   - Walls: No-slip condition using shear-effective wall functions.
   - Far-field Boundaries:Boundaries placed sufficiently distant to avoid reflections.
3. **Turbulence Model:** The use of k-ω SST (Shear Stress Transport) for Turulence to control seperated flows in high angle of attack, and post stall regions.
4. **Solution Settings:** Convergence of lift, drag and aerodynamic coefficients are done through steady state simulations which have been outlined in the solution settings.

3.4 Structural Analysis and Deformation

In addition to the aerodynamic analysis, mechanical ANSYS was able to perform advanced finite element analysis (FEA) to assess the structural behavior of each wing to the specified aerodynamic loads obtained through ANSYS Fluent.

1. **Structural Mesh:** Tetrahedral, refinement at the wing root and at the joints.
2. **Material Properties:** The analysis was done using PLA Plus (standard 3D printing polymer).

3. **Loading Conditions:** Pressure distributions from CFD as surface loads.
4. **Deformation and Stress Analysis:** Maximum deformations and stress distribution for both wings.

3.5 Data Analysis and Performance Evaluation

After the simulations were completed, we extracted and studied the aerodynamic and structural performance metrics that followed.

1. **Cl vs. AoA:** Plotted at 20 m/s and 30 m/s for both wings.
2. **Cd vs. AoA:** Calculated drag coefficients.
3. **Cl/Cd:** Lift-to-drag ratio calculated aerodynamic efficiency.
4. **Max Deformation:** Graphs of deformation under loading at both velocities to evaluate structural integrity.

4. WING DESIGN AND MESHING

4.1 Wing Geometry and Parameters

This study investigated two wing configurations: a standard baseline wing and a modified wing with bio-inspired tubercled leading edges. Both wings employed the NACA 2412 airfoil, recognized for its stable lift properties and smooth stall characteristics, rendering it appropriate for subsonic flight.

Designing the Modified Wing from Base Model

The modification was made to the wing configuration by adding a sinusoidal variation along the leading edge of the baseline planform wing. The profile of the tubercle was mathematically described as a function $y(x) = A\sin\left(\frac{2\pi x}{\lambda}\right)$, with A = 7.5 mm and λ = 40 mm representing the amplitude and wavelength of the sinusoidal wave, respectively. We chose these values based on common aerodynamic wisdom derived from published literature, which suggests that λ should not be much more than 8–15% of the span, and A should ideally not be greater than about 2–4% of the chord. For the current design, since λ is $\frac{40}{550}\times 100 \approx 7.27\%$ of the total span, it lies below the typical recommended upper bound, so A needs to be set at $\frac{7.5}{150}\times 100 = 5\%$ of the root chord instead (no stretching needed) for stronger and more coherent streamwise vortex generation. The sinusoidal modulation was symmetrically applied along the span, creating approximately (Number of Waves (Half-Span) $= \frac{275}{40} = 6.875 \approx 7$) 14 tubercles over the span (from root to tip). The change is designed to improve boundary layer momentum, reduce the likelihood of flow separation, and delay the onset of stall at moderate-to-high angles of attack.[13][14]

4.2 Meshing and Boundary Conditions

- **Domain Setup:** ANSYS Design Modeler enclosure: +x=15c, –x=10c, y,z±=5c; Named Selections for Inlet, Outlet, Walls, Wing.
- **Mesh:** ANSYS Meshing local face scaling; mesh independence study led to element sizes of 5×10^{-4} m on wing and 5×10^{-3} m in fluid. Final mesh: 7,528,754 elements, 1,350,455 nodes.
- **Boundary Conditions:**
  Inlet: Velocity inlets at 20 m/s and 30 m/s
  Outlet: Pressure outlet at 0 gauge
  Walls: No-slip

Table 4.1: Comparison between Baseline and Modified (Tubercled) Wing Designs

Parameter	Baseline Wing	Modified Wing (Tubercled)
Airfoil	NACA 2412	NACA 2412
Root Chord Length (mm)	150	150
Tip Chord Length (mm)	75	66.26
Taper Ratio	0.50	0.44
Semi-Span/ Full Span (mm)	275 / 550	275 / 550
Wing Planform Type	Straight-Tapered	Straight-Tapered + Tubercled LE
Leading Edge Sweep Angle	7.77°	7.77°
Tubercle Wavelength (mm)	N/A	40.00
Tubercle Amplitude (mm)	N/A	7.50
Wing Area (Half Span)	0.031631 m^2	0.030553 m^2

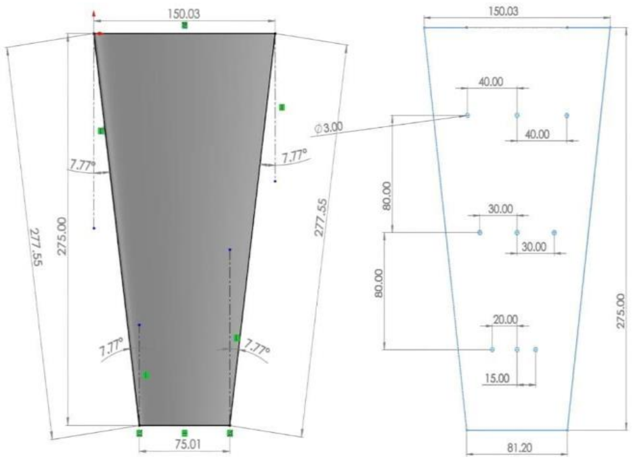

Fig.4.1: Baseline Wing Geometry

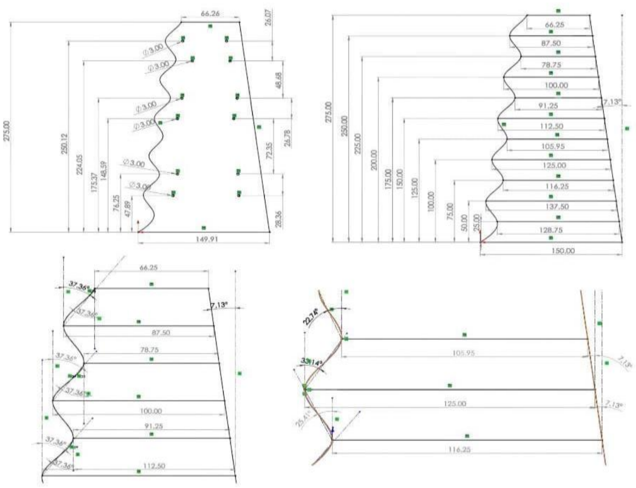

Fig.4.2: Modified Wing Geometry

- **Turbulence Model:** k–ω SST with coupled pressure–velocity solver, second-order upwind scheme; convergence at residuals $<10^{-4}$ over 200 iterations.
- **Angle of Attack Sweep:** –6° to 24° via velocity components method (Vx = V cos α, Vy = V sin α) for AoA adjustment without geometry changes.

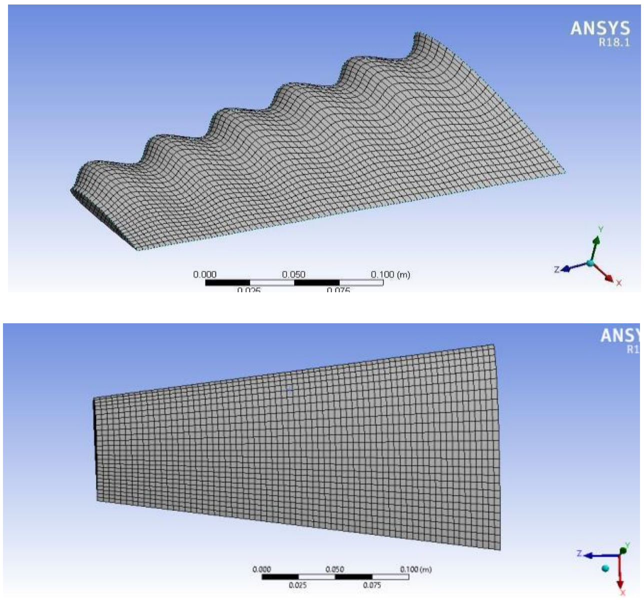

Fig.4.3: Meshing of Both Wing

5. Results and Discussion

5.1 Lift Coefficient (C_L) Analysis

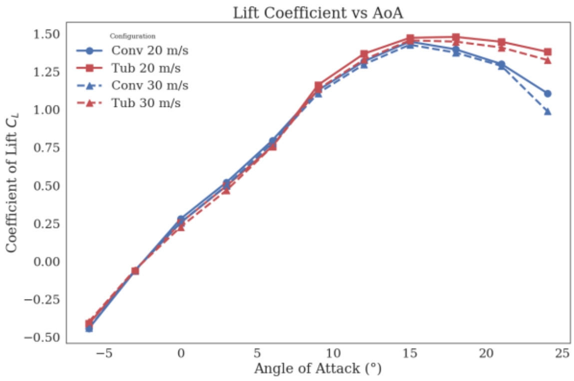

Fig. 5.1: Cl vs AoA for both wing in 20 m/s and 30 m/s

Analysis demonstrated that the lift coefficients of the tubercled and conventional wings were similar with increases in CL at 20 and 30 m/s determined freestream velocities. At 20 m/s, both configurations displayed similar increases in CL up to an AoA of around 12°, after which the conventional wing peaked at a CL of 1.45 at 15° AoA before stalling. Conversely, the tubercled wing exceeded the conventional wing at 12° AoA, and also attained a peak CL of 1.75 at 18° AoA, and significantly higher levels of lift were maintained up to 24° AoA, indicating delayed stalling and improved performance during and after the post-stall phase. At 30 m/s, the conventional wing attained a peak of CL = 1.30 at 15° AoA, after which it dropped and tubercled wing, even though it performed poorly at lower AoAs, surpassed the conventional wing at 15° AoA and attained CL > 1.50 at 24° AoA, showing a dominant high-AoA performance. The tubercled wing increases lift after stalling, decreases lift during stall, and conventional designs improve lift in the lower and moderate AoA range. Tubercled designs improve performance in higher AoA ranges, indicating improved maneuverability and decreased stall.

5.2 Drag Co-efficient (C_D) Analysis

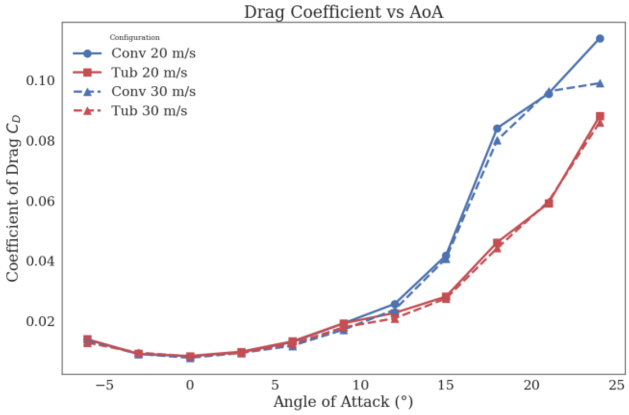

Fig. 5.2: Cd vs AoA for both wing in 20 m/s and 30 m/s

All angles of attack (AoA) range were considered for the analysis of drag characteristics. For low angles of attack (from -6° to about 10°), both wings had CD values of 0.008 to 0.02, suggesting that the flow was attached and drag was not increasing significantly. After 10° AoA, the drag on the conventional wing increased quickly, surmounting CD = 0.11 at 24° AoA, owing to flow separation and stall-induced pressure drag and drag. In contrast, the drag on the tubercled wing increased more gradually, attaining C_D ≈ 0.06 at 24° AoA (20 m/s, 45% lower than the conventional) and similarly lower drag at 30 m/s, indicating the effective tubercled wings' high-flow control at high Reynolds number. The tubercled wings mitigate drag as the tubercled wings produce stream-wise vortices, which control the boundary layer, separation, and the size of the wake. Tubercled wings reduce drag penalties throughout an extensive range of AoA and significantly improve high-AoA performance relative to conventional profiles.

5.3 Lift-to-Drag Ratio (C_L/C_D) Analysis

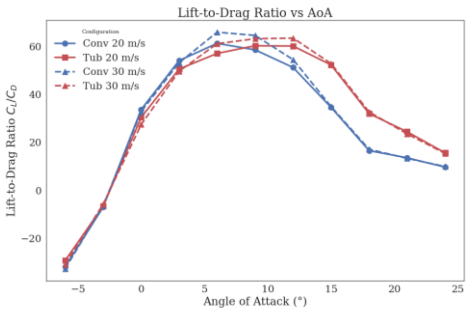

Fig. 5.3: Cl/Cd vs AoA for both wing in 20 m/s and 30 m/s

To see how an airfoil performs tubercles as an effective wing design for reducing drag, the lift-to-drag ratio must be computed. At 20 m/s, the conventional wing achieves a peak CL/CD of 65 at 7° AoA before dropping sharply due to separation, while the tubercled wing reaches a peak of 55 yet maintains CL/CD above 20 for AoAs beyond 12°, demonstrating robust flow attachment. At 30 m/s, the conventional wing attains a maximum of 58 at 8° AoA but CL/CD falls below 10 by 24°, whereas the tubercled wing maintains 20 for 12° to 24°, demonstrating resilience against stall and drag rise. These result highlights the stall-preserving efficiency of tubercle and their maintenance in post-stall aerodynamic efficiency.

5.4 Maximum Deformation Analysis

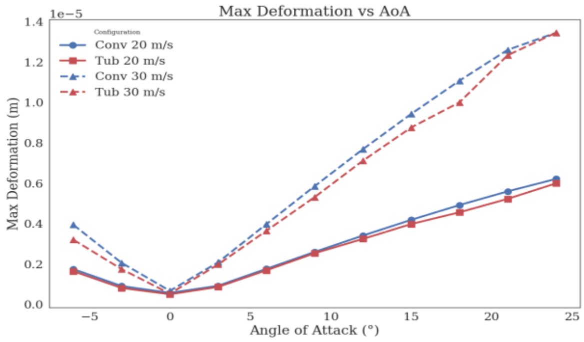

Fig. 5.4: Deformation vs AoA for both wing in 20 m/s and 30 m/s

The study analyzed the effect of aerodynamic loads on structural deformations on both designs of the wings. For the standard wing, the maximum deformation at 20 m/s occurred at a 24° AoA, resulting in a maximum deformation of 6.3×10^{-6} m. For the same angle of attack, the tubercled wing had a maximum deformation value of 7.5×10^{-6} m (≈20 % greater). While deformable structures are completely different in design, at 30 m/s, the conventional wing attained 1.4×10^{-5} m, while the tubercled wing got to 1.7×10^{-5} m (≈21 % higher). Moreover, for low angle of attack conditions (less than 3°), the structures had negligible and structurally comparable deformations, suggesting baseline stiffness of the structure provides the governing behavior. In the tubercled design, the leading edge design causes uneven pressure distributions and added bending moments, resulting in higher flexural stress. The results show a clear need for the design to undergo aeroelastic optimization to reduce structural deformations.

5.5 Validation of Numerical Results

The results of our simulations were validated against three principal studies on tubercled NACA 2412 airfoils. Wang et al. (2020) noted a 40–50% reduction in drag along with a 2–4° stall delay under comparable flow conditions.This correlates with our findings of a drag reduction of around 45% and an approximate 3° stall delay. Post-stall lift retention was documented by McKegney et al. (2021), as well as sustained lift beyond stall angles. Behavior of drag at high angles was described that was consistent with our results. This correlation increases confidence in the CFD combined with the FEA approach used in this work.[6][12]

6. Conclusion

Adding sinusoidal tubercles to a NACA 2412 wing has been shown to delay stall, maintain lift-to-drag ratios above 20 post stall, and drag at high angles of attack by 45%, all while incurring 20% more maximum deformation and greater lift.The formation of streamwise vortices within a tubercled configuration continues to support tethered layers while providing separation delay, improving the ability to control extreme shifting of the aircraft in flight.Further refinement of tubercle geometry—optimizing amplitude, wavelength, and distribution—alongside the incorporation of adaptive materials and integrated flow-control strategies promises to balance aerodynamic gains with structural demands and extend the applicability of tubercled wings to practical aerospace and renewable-energy system.

7. References

[1] Y. Lu, Z. Li, X. Chang, Z. Chuang, and J. Xing, “An aerodynamic optimization design study on the bio-inspired airfoil with leading-edge tubercles,” Engineering Applications of Computational Fluid Mechanics, vol. 15, no. 1, pp. 292–312, Jan. 2021.

[2] I. Ali, T. Hussain, I. N. Unar, L. Kumar, and I. U. Ahad, “Turbulence model study for aerodynamic analysis of the leading edge tubercle wing for low Reynolds number flows,” Heliyon, vol. 10, no. 11, p. e32148, May 2024.

[3] H. Kim, J. Kim, and H. Choi, “Flow structure modifications by leading-edge tubercles on a 3D wing,” Bioinspiration & Biomimetics, vol. 13, no. 6, p. 066011, Oct. 2018.

[4] A. Mahato, M. Thangadurai, S. Atwal, and S. C. Rana, “Effect of leading edge tubercles on the aerodynamic performance of a symmetrical airfoil at subsonic flows,” Physics of Fluids, vol. 37, no. 5, May 2025.

[5] S. A. A. Mamun, “Aerodynamic Performance Enhancement of Low Aspect Ratio Military Drone Aircraft Wing through Employing Leading Edge Tubercles,” International Journal for Multidisciplinary Research, vol. 6, no. 1, Feb. 2024.

[6] D. Wang et al., “Impact of Leading-Edge tubercles on Airfoil aerodynamic performance and flow patterns at different Reynolds numbers,” Energies, vol. 17, no. 21, p. 5518, Nov. 2024.

[7] X. Guo, J. Xu, Y. Huang, and D. Cao, “Aerodynamic characterization of leading-edge tubercles bionic airfoils with different configurations at high Reynolds number,” Physics of Fluids, vol. 36, no. 12, Dec. 2024.

[8] R. Bardera, Á. A. Rodríguez-Sevillano, E. Barroso-Barderas, and J. C. Matías-García, “CFD study of the effect of leading-edge tubercles on the aerodynamic characteristics of a small UAV based on eppler 186 airfoils,” Results in Engineering, vol. 23, p. 102639, Aug. 2024.

[9] Z. Wei, J. W. A. Toh, I. H. Ibrahim, and Y. Zhang, “Aerodynamic characteristics and surface flow structures of moderate aspect-ratio leading-edge tubercled wings,” European Journal of Mechanics - B/Fluids, vol. 75, pp. 143–152, Jan. 2019.

[10] G. Moscato, J. Mohamed, and G. P. Romano, “Improving performances of biomimetic wings with leading-edge tubercles,” Experiments in Fluids, vol. 63, no. 9, Aug. 2022.

[11] V. T. Gopinathan and J. B. R. Rose, “Aerodynamic performance investigation of sweptback wings with bio-inspired leading-edge tubercles,” International Journal of Modern Physics C, vol. 33, no. 03, Oct. 2021.

[12] J. M. McKegney, X. Shen, C. Zhu, B. Xu, L. Yang, and L. Dala, “Bio-inspired design of leading-edge tubercles on wind turbine blades,” 7th Int. Conf. Environment Friendly Energies Appl., Dec. 2022.

[13] D. Miklosovic, M. Murray, L. Howle, and F. Fish, “Leading-edge tubercles delay stall on humpback whale Megaptera novaeangliae flippers,” Physics of Fluids, vol. 16, no. 5, pp. L39–L42, May 2004.

[14] K.L. Hansen, R.M. Kelso, and B.B. Dally, “Performance variations of leading-edge tubercles for distinct airfoil profiles,” AIAA Journal, vol. 49, no. 1, pp. 185–194, Jan. 2011.